Contact Analysis and Mathematical Modeling of Traveling Wave Ultrasonic Motors

Meiling Zhu

***Abstract*—An analysis of the contact layer and a mathematical modeling of traveling wave ultrasonic motors (TWUM) are presented for the guidance of the design of contact layer and the analyses of the influence of the compressive force and contact layer on motor performance. The proposed model starts from a model previously studied but differs from that model in that it adds the analysis of the contact layer and derives the steady-state solutions of the nonlinear equations in the frequency domain, rather than in the time domain, for the analyses of vibrational responses of the stator and operational characteristics of the motor. The maximum permissible compressive force of the motor, the influences of the contact layer material, the thickness of the contact layer, and the compressive force on motor performance have been discussed. The results show that by using the model, one can understand the influence of the compressive force and contact layer material on motor performance, guide the choice of proper contact layer material, and calculate the maximum permissible compressive force and starting voltage.**

I. Introduction

In the last two decades, considerable progress has been achieved in the development of traveling wave ultrasonic motors (TWUM). Several detailed reviews [1]–[3] have been published that describe a range of constructions and their operating principles and characteristics. The motors consist of a stator that uses piezoelectric elements to excite vibrations with a frequency in the ultrasonic range and a rotor (rotary motors) or a slider (linear motors) that is driven by a stator via frictional force. Depending on the geometry of the stator, generally two orthogonal vibrations (e.g., two bending vibrations) are superimposed on an elliptical motion on the contact surface between the stator and the rotor. The high-frequency and small-amplitude vibrations then are rectified by friction force into a lower-frequency macroscopic rotation of the rotor or a linear motion of the slider.

The operational performance of the motor (e.g., output speed, torque, power, and efficiency) are determined mainly by the contact layer material and the compressive force applied on the rotor. To design a TWUM, it would be valuable to have a mathematical model of the motor that takes account of the contact interface, guide a proper choice of contact layer material and understand the influence of the compressive force and the contact layer material on motor performance. Furthermore, it would be useful for a priori calculation of motor characteristics, such as no-load speed, stall torque, maximum permissible compressive force, starting up voltage, input power, output power, and efficiency.

During the last decade, many modeling methods have been proposed for TWUM. The equivalent electric circuit method [4], [5] provides an academically pleasing analysis tool in many fields, but it is not a very useful design tool for TWUM because it does not accurately model the interface forces: the normal compressive and tangential frictional forces. For example, the frictional force is represented by a large parallel sequence of resistors and diodes, the values of which have little physical interpretation. In addition, the integration of the interface forces over finite contact regions is not addressed, and the interaction between the interface forces and the vibrations of the stator is not included. The finite element method (FEM) has been developed for the vibrational analysis of piezoelectric structures [6], and the steady-state performance analysis of the TWUM [7]. The FEM was extended to the analysis of a transient response for three-dimensional (3-D) piezoelectric composite structures. It was shown that this could be applied to TWUM [8]. However, the contact between stator and rotor was not fully taken into account in [7] and [8]. In addition, a detailed finite element (FE) analysis of the contact surface was presented in [9], but the interaction between the interface forces and the vibrations of the stator was not considered. Experimental techniques [10] provided an interesting method for the determination of the motor characteristics, such as stall torque, dynamic frictional coefficient at the contact interface, torque-speed and efficiency-speed characteristics; but the experimental technique cannot easily and effectively be used during preliminary design. Many analytical models of TWUM have been published in the literature [11]–[18]. Most early literature divided the modeling of TWUM into two steps. Using either analytical methods [11] or FEM [6]–[8], [19]–[22], the motor vibration was modeled for the determination of the mode shape, the resonant frequency, and the vibration amplitude. Then, under the assumption that the stator vibrations are not affected by the interface forces and using an analytical model [12]–[15], or equivalent electric circuit [5], [23], or FEM [7], [9], the steady-state or transient characteristics was modeled. Strictly speaking, such a separation is not perfect because the effects of the contact forces on the stator vibration are not well considered.

Manuscript received October 30, 2002; accepted January 16, 2004.
The author is with the Institut B für Mechanik, Stuttgart Universität, Pfaffenwaldring 9, D-70569, Stuttgart, Germany; the School of Industrial and Manufacturing Science, Cranfield University, Bedfordshire, MK43 0AL, UK; and the Institute of Vibration Engineering Research, Nanjing University of Aeronautics & Astronautics, Nanjing, 210016, China (e-mail: m.zhu@cranfield.ac.uk).

0885–3010/$20.00 © 2004 IEEE

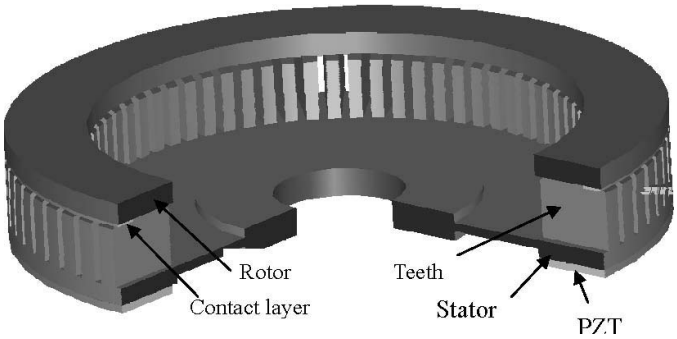

Fig. 1. Geometry of the stator.

The motor that has the component elements (stator, rotor, and contact interface) should be considered as a coupled dynamic system. More recent literature has paid great attention to this deficiency. For example, in [16], the contact forces were calculated and a mathematical model was presented, which was developed into a design tool of TWUM. A mathematical model, which incorporates the rotor flexibility into the model [16], was developed in [17]. A similar model was proposed for the prediction of the input and output characteristics of the TWUM in [18]. Another modeling method, which integrates equivalent electric circuit, FEM, and mathematical modeling was developed in [24]. Furthermore, based on the model [24], an optimized drive control for inverter-fed ultrasonic motors was proposed [25].

However, a mathematical model that can guide the choice of the contact-layer material and can be useful to understanding the operational characteristics of the motor under the action of a compressive force has not yet been developed. In this paper, a contact-layer analysis and a mathematical model of the TWUM is presented for these purposes. The model developed here gives insight into the influences of the compressive forces and the contact-layer material on operational characteristics. The analysis of contact layer is based on the consideration of contact-layer deformation, strain, and stress within it. A mathematical model proposed starts from the model previously studied by Hagood [16] but differs from the Hagood model in that it adds the analysis of the contact layer and steady-state solutions of the nonlinear equations are derived in the frequency domain, rather than in time domain, for the analyses of the vibrational responses of the stator and operational characteristics of the motor. Using the model can guide the choice of proper contact-layer material, the design of the dimensions, and the prediction of the maximum permissible compressive force and starting-up voltage of the TWUM.

II. Description of the Motor

A detailed description of the configuration and the working principle of TWUM can be found in the literature [1], [2]. A 3-D view is shown in Fig. 1. The motor consists of a rotor and a stator to which a piezoceramic ring, which excites a traveling wave, is bonded. A contact layer, which greatly affects the motor performance, is bonded to the rotor. The piezoceramic ring is divided into two parts, each part consisting of a number of sectors with alternating polarizations. By applying two electric fields with a phase shift of 90 degrees to the piezoceramic ring, two orthogonal bending vibrations with the same eigenfrequencies and the same number of nodal diameters can be simultaneously excited in the stator. As a result, a flexural traveling wave is formed. When the flexural traveling wave propagates along the stator circumference, the particles on the stator surface perform elliptical motions. Under the action of a compressive force, the rotor contacts the stator surface and obtains the vibration speed of surface particles in the tangential direction; as a result, the rotor rotates.

III. Contact Analysis

The deformation and distributions of stresses of the contact layer under the action of a compressive force are derived in this section. For simplicity, the following assumptions have been made during the contact analysis:

- The stator is assumed to be a rigid body with a bending profile.
- The contact layer is assumed to have no mass without dissipation.
- Although the contact layer is circular, it is treated as a straight beam because its width is much smaller than its radius.

The contact interface between the stator and the rotor is schematically shown in Fig. 2, where $2a$, d, h_c, P, λ represent the contact length, the penetration of the stator into the contact layer, the thickness of the contact layer, the compressive force, and the wavelength of the traveling wave, respectively.

Under the action of a compressive force P, the rotor contacts the stator surface over areas centered on the wave crests of the traveling wave. Therefore, these contact areas are distributed and move along with the traveling wave. It is advantageous to introduce two coordinate systems into the analysis, one for the x, y, z coordinate system moving with the traveling wave, the other for the $\tilde{x}, \tilde{y}, \tilde{z}$ coordinate system fixed to the stationary stator shown in Fig. 2. The relationship between the two coordinate systems is:

$$\frac{2\pi}{\lambda}x = \frac{2\pi}{\lambda}\tilde{x} - \omega t, \quad y = \tilde{y}, \quad z = \tilde{z}, \tag{1}$$

where ω is the angular frequency of the traveling wave and t the time. As a result, the contact areas are stationary relative to the x, y, z coordinate system.

When the piezoceramic ring is subjected to an electrical field, a traveling wave can be excited in the stator. The expression is:

$$w_{s_0}(r, \tilde{\theta}, t) = W(r)\cos\left(\frac{2\pi r}{\lambda}\tilde{\theta} - \omega t\right), \tag{2}$$

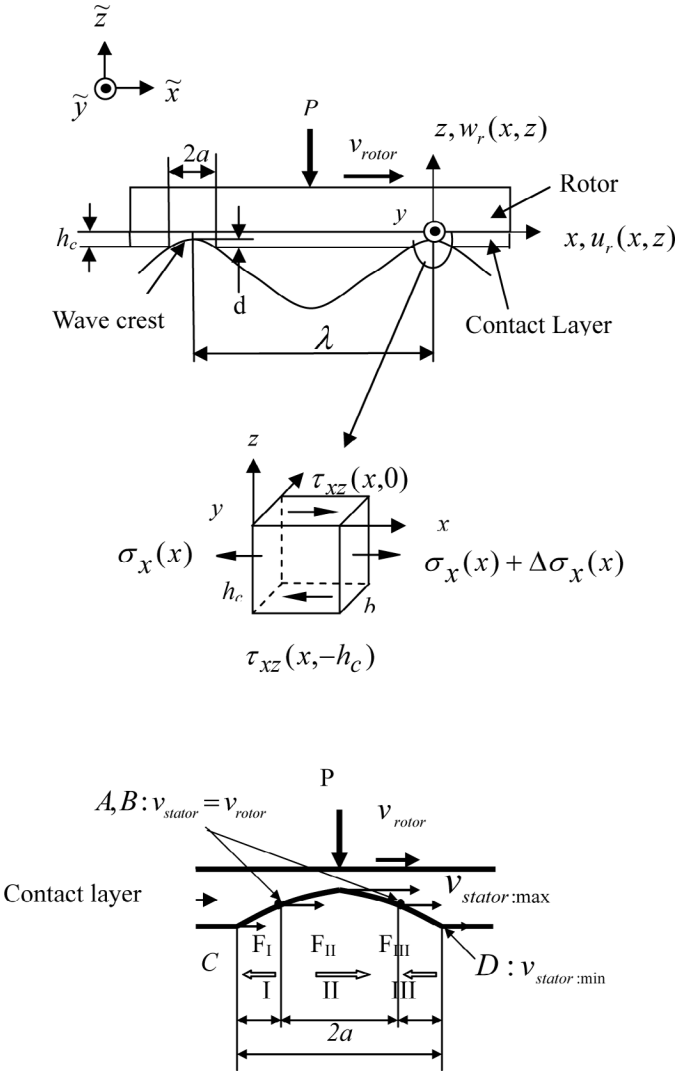

Fig. 2. Contact interface.

where $w_{s_0}(r,\tilde{\theta},t)$ is the out-of-plane displacement of the midplane of the stator with $\tilde{\theta}=\frac{\tilde{x}}{r}$ and $r=y$, and the subscript s denotes the stator, and $W(r)$ is the amplitude of the traveling wave at arbitrary radius r of the stator.

Under the action of the compressive force, the deformation of the contact layer can be expressed as shown in (3) (see next page), where $\delta(R,x)$ is the deformation at contact radius R, $d=W(R)\left(1-\cos\frac{2\pi}{\lambda}a\right)$ and d_0 is the initial contact deformation of the contact layer under the action of P and is given by $d_0=\frac{1}{2G}\frac{1-2\nu}{1-\nu}\frac{h_c}{S}P$ with ν, G, S being the Poisson's ratio, the shear modulus, and the contact area of the contact layer. Whether the rotor is able to rotate depends on the input voltage. Without input voltage on the piezoceramic ring, clearly $W(R)=0$, so there is no movement. For an input voltage less than V_S, the starting-up voltage under the action of P, $W(R)<\frac{d_0}{2}$, the rotor cannot rotate. However, for an input voltage larger than V_S, $W(R)>\frac{d_0}{2}$, the rotor may be able to rotate depending on the value of the compressive force.

Using the displacement functions commonly used in mechanics, the stress and strain distributions in the contact layer can be obtained. The displacement functions can be [26]:

$$\begin{aligned} u_r(x,z) &= A(x)+B(x)z,\\ w_r(x,z) &= J(x)+L(x)z, \end{aligned} \tag{4}$$

where $u_r(x,\,z)$ and $w_r(x,\,z)$ represent the tangential and local normal displacements of the contact layer, with the subscript r denoting the rotor and are not functions of y as the contact layer is treated as a straight beam due to its narrow width. $A(x)$, $B(x)$, $J(x)$, and $L(x)$ are the functions determined in the following.

The contact layer is bonded to the substrate of the rotor, so $u_r(x,0)=0$ and $w_r(x,0)=0$ at $z=0$. As a result, $A(x)=0$, $J(x)=0$ and:

$$\begin{aligned} u_r(x,z) &= B(x)z,\\ w_r(x,z) &= L(x)z, \end{aligned} \tag{5}$$

where $L(x)$ is determined by the expression: $w_r(x,-h_c)=-\delta(R,x)$, and

$$L(x)=-\frac{d-W(R)\left(1-\cos\frac{2\pi}{\lambda}x\right)}{h_c}, \qquad \text{if } W(R)>d_0,\ \ a<\frac{\lambda}{2}, \tag{6}$$

where $B(x)$ is obtained from the following relationships and derivations.

The relationships between the strains and the displacement functions are:

$$\begin{aligned} \epsilon_x(x,z) &= \frac{\partial u_r(x,z)}{\partial x}=\frac{\partial B(x)}{\partial x}z,\\ \epsilon_z(x,z) &= \frac{\partial w_r(x,z)}{\partial z}=L(x),\\ \gamma_{xz}(x,z) &= \frac{\partial u_r(x,z)}{\partial z}+\frac{\partial w_r(x,z)}{\partial x}=B(x)+\frac{\partial L(x)}{\partial x}z, \end{aligned} \tag{7}$$

when $z=0$ and $z=-h_c$:

$$\begin{aligned} \gamma_{xz}(x,0) &= B(x),\\ \gamma_{xz}(x,-h_c) &= B(x)-\frac{\partial L(x)}{\partial x}h_c. \end{aligned} \tag{8}$$

The relationships between the averaged stresses and strains are:

$$\begin{aligned} \bar{\sigma}_x(x) &= \frac{2\nu G}{1-2\nu}[\bar{\epsilon}_x(x)+\bar{\epsilon}_y(x)+\bar{\epsilon}_z(x)]+2G\bar{\epsilon}_x(x),\\ \bar{\sigma}_y(x) &= \frac{2\nu G}{1-2\nu}[\bar{\epsilon}_x(x)+\bar{\epsilon}_y(x)+\bar{\epsilon}_z(x)]+2G\bar{\epsilon}_y(x),\\ \bar{\sigma}_z(x) &= \frac{2\nu G}{1-2\nu}[\bar{\epsilon}_x(x)+\bar{\epsilon}_y(x)+\bar{\epsilon}_z(x)]+2G\bar{\epsilon}_z(x),\\ \tau_{xz}(x,0) &= G\gamma_{xz}(x,0)=GB(x)\\ \tau_{xz}(x,-h_c) &= G\gamma_{xz}(x,h_c)=G\left[B(x)-\frac{\partial L(x)}{\partial x}h_c\right], \end{aligned} \tag{9}$$

where $\bar{\sigma}_x(x)$, $\bar{\sigma}_y(x)$, and $\bar{\sigma}_z(x)$ are the averaged stresses of the contact layer; $\tau_{xz}(x,0)$, $\tau_{xz}(x,-h_c)$ and $\gamma_{xz},(x,0)$,

$$\delta(R,x)=\begin{cases}-d_0, & \text{When } W(R)=0,\ a=\frac{\lambda}{2},\\ -\left[d_0+W(R)\cos\frac{2\pi}{\lambda}x\right], & \text{When } W(R)<\frac{d_0}{2},\ a=\frac{\lambda}{2},\\ -\left[d-W(R)\left(1-\cos\frac{2\pi}{\lambda}x\right)\right], & \text{When } W(R)>\frac{d_0}{2},\ a<\frac{\lambda}{2},\end{cases} \tag{3}$$

$\gamma_{xz}(x,-h_c)$ are the shear stresses and strains, respectively, acting on the $z=0$ and $z=-h_c$ surfaces; $\bar{\epsilon}_x(x)$, $\bar{\epsilon}_y(x)$ and $\bar{\epsilon}_z(x)$ are the averaged strains and:

$$\bar{\epsilon}_x(x)=\frac{1}{h_c}\int_{-h_c}^{0}\epsilon_x(x,z)dz=-\frac{h_c}{2}\frac{\partial B(x)}{\partial x},\ \bar{\epsilon}_z(x)=L(x), \tag{10}$$

with assumption that $\bar{\epsilon}_y(x)=0$.

Because $a/h_c\gg 1$, using the stress analysis, as shown in Fig. 2, yields the following equilibrium equation of the contact layer in the x direction:

$$\frac{d\bar{\sigma}_x(x)}{dx}=\frac{\tau_{xz}(x,-h_c)-\tau_{xz}(x,0)}{h_c}. \tag{11}$$

Substitution of (9) into (11) yields:

$$h_c(1-\nu)\frac{\partial^2 B(x)}{\partial x^2}=\frac{\partial L(x)}{\partial x}. \tag{12}$$

Solving (12) gives:

$$B(x)=-\frac{W(R)\lambda}{2\pi h_c^2(1-\nu)}\sin\frac{2\pi}{\lambda}x+c_1x+c_2,\quad \text{if } W(R)>d_0,\ a<\frac{\lambda}{2}, \tag{13}$$

where c_1 and c_2 are integrated constants determined by the boundary conditions at $(x,z)=(\mp a,-h_c)$. Because $\bar{\epsilon}_z(\mp a)=0$, substitution of (13) into (10) yields $c_1=\frac{1}{h_c^2(1-\nu)}W(R)\cos\frac{2\pi}{\lambda}a$. With $p(x)$ denoting the distribution of the normal compressive stress within the contact regions, then:

$$p(x)=\bar{\sigma}_z(x)=-k_nW(R)\left(\cos\frac{2\pi}{\lambda}x-\cos\frac{2\pi}{\lambda}a\right),\quad \text{if } W(R)>d_0,\ a<\frac{\lambda}{2} \tag{14}$$

where $k_n=\frac{2\nu^2-3\nu+2}{(1-2\nu)(1-\nu)}\frac{G}{h_c}$. The resultant of the distribution of the normal compressive forces is given by:

$$\begin{aligned}P&=n\int_{-a}^{a}p(x)bdx\\&=-2nbk_nW(R)\left(\frac{\lambda}{2\pi}\sin\frac{2\pi}{\lambda}a-a\cos\frac{2\pi}{\lambda}a\right),\\&\quad \text{if } W(R)>d_0,\ a<\frac{\lambda}{2},\end{aligned} \tag{15}$$

where n is the number of wavelengths along the stator and b is the contact width between the stator and the rotor.

The tangential stress $\tau(x)$ is equal to $\tau_{xz}(x,-h_c)$ and:

$$\tau(x)=GW(R)\left\{-\left[\frac{1}{\frac{2\pi}{\lambda}h_c^2(1-\nu)}+\frac{2\pi}{\lambda}\right]\sin\frac{2\pi}{\lambda}x+\frac{1}{h_c^2(1-\nu)}x\cos\frac{2\pi}{\lambda}a+c_2\right\},\quad \text{in the case of no slipping;} \tag{16}$$

$$\tau(x)=\mu\, sign\, p(x),\quad \text{in the case of slipping,}$$

where μ is the frictional coefficient and $sign$ is the sign function.

Outside the contact regions, $p(x)=\tau(x)=0$.

IV. Model of the Stator

This section will start from the Hagood [16] model and derive nonlinear governing equations of motion of the stator. But the model derived here differs from the Hagood model in that it adds the analysis of the contact layer, and steady-state solutions of the nonlinear equations are derived in the frequency domain, rather than in time domain, for the analyses of the vibrational responses of the stator and operational characteristics of the motor. Using the model, the maximum permissible compressive force and starting-up voltage of the TWUM is given in the section.

According to [27], the generalized Hamilton's principle can be written as:

$$\int_{t_0}^{t_1}\int_{V_s+V_p}(\delta H-\delta K)dvdt=\int_{t_0}^{t_1}\left[\int_{V_s+V_p}G_i\delta u_i+\int_S(f_i\delta u_i+q_i\delta\phi_i)ds\right]dt, \tag{17}$$

where t_0 and t_1 are the two arbitrary time, δ is the variation operator, H is the electric enthalpy, K is the kinetic energy, G_i is the body force, f_i is the traction along the boundary surface, q_i is the electric charge, u_i is the component of the displacement vector of the stator, ϕ_i is the electric potential, and $i=1$, 2 and 3. V_s+V_p denotes the entire domain of the volume of the stator with s and p, respectively, denoting the substrate of the stator and the piezoceramic ring, and S denotes the boundary of the domain. The terms on the right-hand side of (17) are the virtual work.

The electric enthalpy H is defined as:

$$H = U_0 - D_i E_i, \tag{18}$$

where U_0 is the internal energy, E_i and D_i are the electric field and the electric displacement, respectively.

The variation of H is:

$$\delta H(\{\varepsilon\}, \{E\}) = \{\sigma\}^T \delta\{\varepsilon\} - \{D\}^T \delta\{E\}, \tag{19}$$

where $\{\varepsilon\}$ is the strain vector, $\{E\}$ is the electric field vector, $\{\sigma\}$ is the stress vector, and $\{D\}$ is the electric displacement vector.

The kinetic energy K is defined as:

$$K = \frac{1}{2}\{\dot{u}_i\}^T \rho \{\dot{u}_i\}, \tag{20}$$

where $\{\dot{u}_i\}$ is the velocity vector of the stator and ρ is the density of the stator.

Because the structure of the stator under consideration is a thin plate, according to elastic mechanics, the plate is considered to be under plane stress. In addition, the polarization of the piezoelectric ring is in the z direction, and the voltages are only applied to the polarized direction. Therefore, the electric field and the electric displacement are nonzero in the z direction only. As a result, $\{E\} = E_3$ and $\{D\} = D_3$.

The constitutive equations for piezoelectric material under plane stress are:

$$\begin{aligned} \{\sigma\} &= [c_p]\{\varepsilon\} - [e]^T E_3, \\ D_3 &= [e]\{\varepsilon\} + \epsilon_p E_3, \end{aligned} \tag{21}$$

where $\{\sigma\} = \{\sigma_r, \sigma_\theta, \tau_{r\theta}\}^T$, $[c_p]$ is the elastic constant matrix of the piezoelectric material, $\{\varepsilon\} = \{\varepsilon_r, \varepsilon_\theta, \gamma_{r\theta}\}^T$, $[e]$ is the piezoelectric constant matrix and $[e] = [e_{31}, e_{31}, 0]$, and ϵ_p is the dielectric constant.

The constitutive equations for the substrate of the stator are:

$$\{\sigma\} = [c_s]\{\varepsilon\}, \tag{22}$$

where $[c_s]$ is the elastic constant matrix of the substrate of the stator.

Substituting (21) and (22) into (19) gives (23) (see next page) where, for the PZT layer, the first term on the right-hand side is the variation of the elastic strain energy of the PZT layer, the second and third terms are the variations of the electromechanical coupling energy, and the fourth term is the variation of the electric energy; for the stator substrate there is the variations of the elastic strain energy only.

For the virtual work on the right-hand side in (17), the first term is zero because $G_i = 0$, and the second term is equal to the sum of the variations of the normal work and the tangential work. The effect of the tangential traction upon the out-of-plane vibration of the stator is rather small, which had been confirmed by the simulation results in [16]. The simulation results are understandable and can be physically interpreted. Because the tangential traction is vertical to the out-of-plane vibration of the stator, the work done by the tangential traction is equal to zero. In addition, the tangential traction has a different sign in the contact region, part of work done by the tangential traction is partly canceled by each other. Therefore, neglect the tangential work term and merely consider the normal work term in the governing equations of motion of the stator. The variation of the normal work is:

$$\delta W_n = nb \int_{\omega t - 2\pi a/\lambda}^{\omega t + 2\pi a/\lambda} p(\hat{x}) \delta w_{s_0}(R, \hat{x}, t) d\hat{x}. \tag{24}$$

The third term is $\int_S q_i \delta\phi_i ds = \int_S q_3 \delta\phi_3 ds$.

Due to small, in-plane inertia, it is assumed that in-plane displacements of the midplane are zero, that is, $u_{s_0}(r, \tilde{\theta}, t) = 0$ and $v_{s_0}(r, \tilde{\theta}, t) = 0$. According to the Kirchoff's plate theory, the displacement vector of the stator can be written in the cylindrical coordinate system as:

$$\{u_i\} = \begin{Bmatrix} u_s(r, \tilde{\theta}, z, t) \\ v_s(r, \tilde{\theta}, z, t) \\ w_s(r, \tilde{\theta}, z, t) \end{Bmatrix} = \Phi_{\text{inertia}} w_{s_0}(r, \tilde{\theta}, t), \tag{25}$$

where $\Phi_{\text{inertia}} = \left\{ -z\frac{\partial}{\partial r} \quad -\frac{z}{r}\frac{\partial}{\partial \tilde{\theta}} \quad 1 \right\}^T$. It should be noted that due to $\tilde{\theta} = \frac{\tilde{x}}{r}$, $\tilde{y} = y = r$, $\tilde{z} = z$, the $\tilde{x}$, $\tilde{y}$, $\tilde{z}$ coordinate system is written as the r, $\tilde{\theta}$, z coordinate system.

The relationship between the stator strains and the displacements is:

$$\{\varepsilon\} = \begin{Bmatrix} \varepsilon_r \\ \varepsilon_\theta \\ \gamma_{r\theta} \end{Bmatrix} = L_{\text{mech}} w_{s_0}(r, \tilde{\theta}, t), \tag{26}$$

where $L_{\text{mech}} = \begin{Bmatrix} -z\dfrac{\partial^2}{\partial r^2} \\ -\dfrac{z}{r}\dfrac{\partial}{\partial r} - \dfrac{z}{r^2}\dfrac{\partial^2}{\partial \tilde{\theta}^2} \\ -\dfrac{2z}{r}\dfrac{\partial^2}{\partial r \partial \tilde{\theta}} + \dfrac{2z}{r^2}\dfrac{\partial}{\partial \tilde{\theta}} \end{Bmatrix}$.

If the out-of-plane displacement of the midplane of the stator can be expressed as:

$$w_{s_0}(r, \tilde{\theta}, t) = \Phi_{\text{mech}}(r, \tilde{\theta})\{\xi_i(t)\}, \tag{27}$$

where $\Phi_{\text{mech}}(r, \tilde{\theta}) = \left\{ g(r) \sin n\tilde{\theta} \;\; g(r) \cos n\tilde{\theta} \right\}$, $\{\xi_i(t)\} = \{\xi_1(t) \;\; \xi_2(t)\}^T \cdot g(r)$ is the vibrational shape function in the r direction, $\Phi_{\text{mech}}(r, \tilde{\theta})$ is the vibrational shape function, and $\{\xi_i(t)\}$ is the vector of the generalized out-of-plane displacements of the stator vibration, then:

$$\{\varepsilon\} = N_{\text{mech}}\{\xi_i(t)\}, \tag{28}$$

where N_{mech} is the operator matrix and $N_{\text{mech}} = L_{\text{mech}}\Phi_{\text{mech}}(r, \tilde{\theta})$.

According to the requirements of producing a traveling wave in the stator, the piezoceramic ring is divided into two parts, A and B, with a phase shift of $\frac{\pi}{2}$ in space, and

$$\delta H = \begin{cases} \{\varepsilon\}^T[c_p]\delta\{\varepsilon\} - \{\varepsilon\}^T[e]^T\delta\{E_3\} - E_3[e]\delta\{\varepsilon\} - \epsilon_p E_3 \delta E_3, & \text{for the PZT layer,} \\ \{\varepsilon\}^T[c_s]\delta\{\varepsilon\}, & \text{for the stator substrate,} \end{cases} \tag{23}$$

the ring has three electrodes: one common electrode with an electric potential of zero is bonded to the stator; the other two electrodes are A and B excited by two applied voltages with a phase shift of $\frac{\pi}{2}$.

Furthermore, according to the polarization pattern of the piezoelectric ring, the relationship between the electric potentials, the electrodes shape, and the applied voltages can be written as:

$$\begin{aligned} \phi_3(\tilde{\theta}, z, t) &= \frac{z}{h_p}\left[\Phi_{\text{elec}_A}(\tilde{\theta})\ \Phi_{\text{elec}_B}(\tilde{\theta})\right]\begin{Bmatrix} v_{\text{elec}_A}(t) \\ v_{\text{elec}_B}(t)\end{Bmatrix} \\ &= \frac{z}{h_p}\Phi_{\text{elec}}(\tilde{\theta})\{v_{\text{elec}_i}(t)\}, \quad i = A,\, B, \end{aligned} \tag{29}$$

where $\phi_3(\hat{\theta}, z, t)$ is the electric potential applied on the piezoelectric ring, $\{v_{\text{elec}_i}(t)\}$ is the applied electric voltage vector, h_p is the thickness of the piezoelectric ring, and $\Phi_{\text{elec}_A}(\tilde{\theta})$ and $\Phi_{\text{elec}_B}(\tilde{\theta})$ are the polarization functions of the part A and B of the piezoelectric ring.

The relationship between the electric field $E_3(\tilde{\theta}, z, t)$ and the electric potential $\phi_3(\tilde{\theta}, z, t)$ is:

$$E_3(\tilde{\theta}, z, t) = -\frac{\partial \phi_3(\tilde{\theta}, z, t)}{\partial z} \tag{30}$$

As a result, the relationship between the electric field and the applied electric voltages is:

$$E_3(\tilde{\theta}, z, t) = N_{\text{elec}}(\tilde{\theta})\{v_{\text{elec}_i}(t)\}. \tag{31}$$

where $N_{\text{elec}}(\tilde{\theta}) = -\Phi_{\text{elec}}(\tilde{\theta})$.

Substituting the expression of the virtual work, (20) and (23) into (17), and carrying out variations of the vector $\{\xi_i(t)\}$ and electric voltage vector $\{v_{\text{elec}_i}(t)\}$ result in the nonlinear governing equations for the motion of the stator.

$$\begin{aligned} M_s\{\ddot{\xi}_i(t)\} + C_s\{\dot{\xi}_i(t)\} + K_s\{\xi_i(t)\} \\ = \Theta\{v_{\text{elec}_i}(t)\} + \{F_{gn_i}\} \qquad i = 1, 2. \\ \Theta^T\{\xi_i(t)\} + C_e\{v_{\text{elec}_i}(t)\} = \{q_{3i}(t)\}, \end{aligned} \tag{32}$$

where

$$\begin{aligned} M_s &= M_{V_s} + M_{V_p}, \\ K_s &= K_{V_s} + K_{V_p}, \\ M_{V_s} &= \int_{V_s} (\Phi_{\text{inertia}}\Phi_{\text{mech}})^T \rho_s \Phi_{\text{inertial}}\Phi_{\text{mech}} dv, \\ M_{V_p} &= \int_{V_p} (\Phi_{\text{inertia}}\Phi_{\text{mech}})^T \rho_p \Phi_{\text{inertial}}\Phi_{\text{mech}} dv, \\ K_{V_s} &= \int_{V_s} N_{\text{mech}}^T[c_s]N_{\text{mech}} dv, \\ K_{V_p} &= \int_{V_p} N_{\text{mech}}^T[c_p]N_{\text{mech}} dv, \end{aligned} \tag{33a}$$

$$\begin{aligned} F_{gn_i} &= -2k_n nbg^2(R)\left(a - \frac{\sin\frac{4\pi}{\lambda}a}{\frac{4\pi}{\lambda}}\right)\xi_i(t), \\ C_s &= 2M_s\omega_n\varsigma, \\ C_e &= \int_{V_p} N_{\text{elec}}^T \epsilon_p N_{\text{elec}} dv, \\ \Theta &= \int_{V_p} N_{\text{mech}}^T[e]^T N_{\text{elec}} dv, \end{aligned} \tag{33b}$$

where M_s, C_s, and K_s represent the modal mass matrix, the coefficient matrix of modal damping, and the modal stiffness matrix of the stator, respectively. Every component of M_s, C_s, and K_s is denoted by the corresponding lower case letter as follows: ς is an empirically added damping factor, ω_n is the natural frequency of the stator without action of the compressive force, and $\omega_n = \sqrt{\frac{k_s}{m_s}}$. Θ represents the electromechanical coupling matrix and describes the conversion of the applied electric voltages to equivalent forces on the stator. Therefore, Θ is called the electromagnetic coupling factor matrix. $\{F_{gn_i}\}$ denotes the generalized force vector, C_e is the electric capacity matrix of the piezoelectric ring and $\{q_{3i}(t)\}$ is the electric charge vector produced on the piezoelectric ring surface. Through the calculation for M_s, C_s, K_s, C_e, and Θ, it can be found that the matrices, M_s, K_s, C_s, and C_e, are diagonal. The matrix, Θ, has zero diagonal elements and has nonzero, nondiagonal elements. Taking any one of (32) obtains (34) for derivation of the solutions to the nonlinear governing equations of motion.

$$\begin{aligned} m_s\ddot{\xi}_i(t) + c_s\dot{\xi}_i(t) \\ + \left[k_s + 2k_n nbg^2(R)\left(a - \frac{\sin\frac{4\pi}{\lambda}a}{\frac{4\pi}{\lambda}}\right)\right] \\ \xi_i(t) = \Theta_i v_{\text{elec}_j}(t) \\ i = 1,\ j = B;\ i = 2,\ j = A. \end{aligned} \tag{34}$$

Let:

$$\begin{aligned} v_{\text{elec}_A}(t) &= V\cos(\omega t + \varphi), \\ v_{\text{elec}_B}(t) &= V\sin(\omega t + \varphi), \end{aligned} \tag{35}$$

with V being the amplitude of the applied electric voltages and φ the unknown and the amount that the output lags the input. Furthermore, let:

$$\begin{aligned} \xi_1(t) &= A(t)\sin\omega t, \\ \xi_2(t) &= A(t)\cos\omega t, \end{aligned} \tag{36}$$

where $A(t)$ is the unknown and a quantity relative to the amplitude of the traveling wave. Because only the steady-state solution of the stator vibration is discussed here, $A(t)$ is independent of time and denoted by A. From (2), (27), and (36), the statement that $W(R,t) = Ag(R)$ can be derived. As a result, $W(R,t)$ also is independent of time and denoted by $W(R)$. Let $\eta = \frac{\omega}{\omega_n}$, substitution of (35) and (36) into (34) obtains the solution as:

$$A = A_0\beta$$
$$\tan\varphi(\eta) = \frac{2\varsigma\eta}{1 + 2nbg^2(R)\left(a - \frac{\sin\frac{4\pi}{\lambda}a}{\frac{4\pi}{\lambda}}\right)\frac{k_n}{k_s} - \eta^2}, \tag{37}$$

where A_0 denotes the static deflection produced by the direct electric voltages, β is the magnification factor of the static deflection in the case of vibration, and:

$$A_0 = \frac{\Theta V}{k_s}$$
$$\beta = \frac{1}{\sqrt{[(1 + 2nbg^2(R)\left(a - \frac{\sin\frac{4\pi}{\lambda}a}{\frac{4\pi}{\lambda}}\right)\frac{k_n}{k_s} - \eta^2]^2 + (2\varsigma\eta)^2}}, \tag{38}$$

where a is the half of contact length and determined by (39).

$$\frac{P}{A_0} = \frac{-2k_n nbg(R)\left(\frac{\lambda}{2\pi}\sin\frac{2\pi}{\lambda}a - a\cos\frac{2\pi}{\lambda}a\right)}{\sqrt{[1 + 2nbg^2(R)\left(a - \frac{\sin\frac{4\pi}{\lambda}a}{\frac{4\pi}{\lambda}}\right)\frac{k_n}{k_s} - \eta^2]^2 + (2\varsigma\eta)^2}}, \tag{39}$$

where (39) is derived from (16) and (37).

As $a \to \frac{\lambda}{2}$, the compressive force P tends to be:

$$P = A_0\frac{-2k_n nbg(R)\frac{\lambda}{2}}{\sqrt{[1 + 2nbg^2(R)\frac{\lambda}{2}\frac{k_n}{k_s} - \eta^2]^2 + (2\varsigma\eta)^2}}. \tag{40}$$

The compressive force in (40) is called the maximum compressive force of the motor and denoted by $P_{\max}$. Because, when the compressive force is larger than the $P_{\max}$, the motor cannot rotate.

In addition, according to the condition that $W(R) > \frac{d_0}{2}$ and (37), a starting-up voltage of the motor (V_s) under the action of a compressive force is obtained and:

$$V_s > \frac{1}{4G}\frac{1-2\nu}{1-\nu}\frac{h_c}{2\pi Rb}\frac{k_s}{\Theta g(R)}$$
$$\sqrt{[(1 + 2nbg^2(R)\left(a - \frac{\sin\frac{4\pi}{\lambda}a}{\frac{4\pi}{\lambda}}\right)\frac{k_n}{k_s} - \eta^2]^2 + (2\varsigma\eta)^2}. \tag{41}$$

V. Performance of the Motor

The rotation of the rotor in a steady-state condition is determined by:

$$C_r\dot{\alpha} = M_{\text{contact}} - M_{\text{applied}}, \tag{42}$$

where C_r is the damping coefficient of the motor, $\dot{\alpha}$ is the angular speed of the rotor, M_{contact} is the torque produced by friction between the stator and the rotor, and M_{applied} is the external load applied to the rotor.

It is assumed that, if the tangential speed of the stator vibration at the contact point differs from the tangential speed of the rotor, slipping occurs. Otherwise, sticking occurs. The frictional force is described by Coulomb's law, that is:

$$f(x) = \mu\, sign\, p(x), \tag{43}$$

where $f(x)$ is the frictional force, μ is the frictional coefficient, and $sign$ is the sign function and:

$$sign = \begin{cases} 1, & \text{if } v_{\text{stator}} > v_{\text{rotor}}, \\ 0, & \text{if } v_{\text{stator}} = v_{\text{rotor}}, \\ -1, & \text{if } v_{\text{stator}} < v_{\text{rotor}}, \end{cases} \tag{44}$$

in which:

$$v_{\text{stator}} = -h_{ct}\frac{2\pi}{\lambda}W(R)\omega\cos\left(\frac{2\pi}{\lambda}x\right), \tag{45}$$

$$v_{\text{rotor}} = R\dot{\alpha}, \tag{46}$$

where v_{stator} and v_{rotor} denote the tangential velocities of the stator and rotor, respectively, h_{ct} denotes the distance from the central layer of the stator to the contact surface. As a result, M_{contact} can be expressed as:

$$M_{\text{contact}} = -2n\mu Rb\int_0^a sign\, p(x)dx. \tag{47}$$

If the speed of the rotor is taken to be:

$$v_{\text{rotor}} = -h_{ct}\frac{2\pi}{\lambda}W(R)\omega\cos\frac{2\pi}{\lambda}x_k, \tag{48}$$

where x_k denotes the point at which the speed of the rotor is equal to the speed of one point of the stator. Through solving (42) and finding the point x_k, the speed of the

TABLE I
MATERIAL PROPERTY PARAMETERS OF THE STATOR.

	Substrate	Piezoelectric ring
Materials	Phosphor bronze	PZT-4
Young's modulus E(GPa)	112	80
Poisson ratio ν	0.33	0.31
Density ρ (kg/m^3)	7790	8790
Piezoelectric constant d_{31}(m/V)	0	-127×10^{-12}
Dielectric constant ε_3 (F/m)	0	1127 ε_0

rotor versus the external load applied to the rotor can be obtained for a steady-state condition. On this basis, many other characteristics of the motors, including the efficiency, the output power, the input power, and the stall torque of the motors can be obtained.

VI. Numerical Results and Discussions

To obtain numerical results from the present model, the shape function, $g(r)$, is introduced:

$$g(r) = a_1 \left(\frac{r - r_i}{r_o - r_i}\right)^2 + a_2 \left(\frac{r - r_i}{r_o - r_i}\right)^3, \qquad (49)$$

where a_1 and a_2 are the coefficients determined by the Rayleigh Ritz method, r_i is the inner-radius of the stator and r_o is the outer-radius of the stator. The function satisfies the geometric boundary conditions at the inner-radius, that is $g(r_i) = 0$ and $g'(r_i) = 0$. The material parameters used here are shown in Table I and the 3-D configuration in Fig. 1.

The piezoceramic ring has the same structure as Shinsei's largest disk type of TWUM and can excite a traveling wave with nine wavelengths. MATLAB (The Math Works, Inc., Natick, MA) software is used for the simulation and the function, *fzero*, which can find a zero of one equation with one variable, is used to solve (39) and (42). The maximum permissible compressive force of the motor, the influences of the contact layer material, the thickness of the contact layer, and the compressive force on motor performance are discussed in this section.

A. Maximum Permissible Compressive Force of the Motor ($P_{\max}$)

The $P_{\max}$ as a function of frequency has been simulated for different contact layer material and is shown in Fig. 3 for specific values of V, h_c, and ς. From Fig. 3, it can be observed that, the Young's modulus of the contact layer material has different influence on the P_{max} in a different frequency range. For $\frac{\omega}{\omega_n} < 1$, the motor system seems to be a static system and the higher value the Young's modulus of the contact layer material, the greater the contact stiffness and the higher the $P_{\max}$. For $\frac{\omega}{\omega_n} > 1$, the motor system seems to be a dynamic system because, in this case,

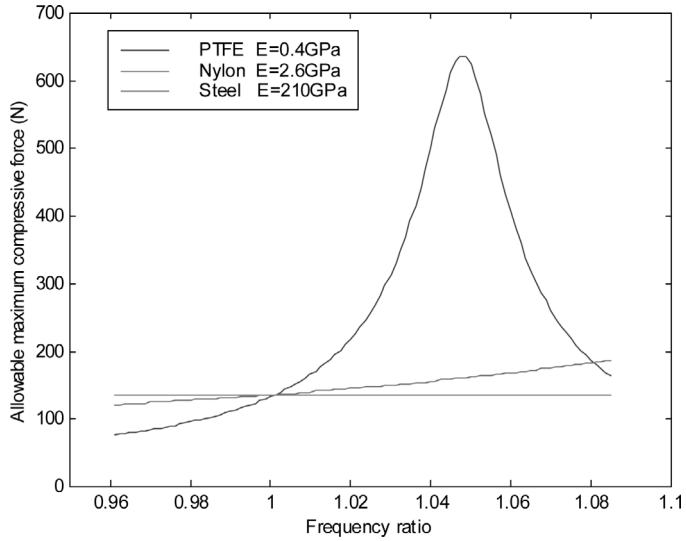

Fig. 3. Maximum permissible compressive forces of the motor where $V = 150$ V, $h_c = 0.5$ mm, and $\zeta = 1\%$.

$P_{\max}$ is determined by the mass, the stiffness of the stator, and the contact layer and the damping. For $\frac{\omega}{\omega_n} > 1$ and near 1, the less the contact stiffness, the higher the $P_{\max}$. The phenomenon is very similar to dynamic design of shafts at high speed in which the lower the stiffness the higher the load the shaft can be subjected to.

B. Influence of the Contact Layer Material on Motor Performance

However, from Fig. 3, it cannot be concluded that the contact layer with a lower Young's modulus always gives improved motor characteristics for $\frac{\omega}{\omega_n} > 1$ and near 1. The frequency responses of the amplitude of the traveling wave of the stator, the contact length between the stator and rotor and rotation speed of the rotor for different contact layer material have been simulated and are shown in Fig. 4 with P, M_{applied}, V, h_c, μ, and ς having values of -80 N, 0.15 Nm, 50 V, 0.5 mm, 0.18 and 1%, respectively. From these figures, it can be seen that the contact layer material only has a small effect on the amplitude of the traveling wave of the stator, but it has great effect on the contact length and the rotation speed of the motor. There is a notch shape of the contact length when the frequency is near to the resonant frequency of the motor system. The main reason is that, when the motor system works near to the resonant frequency, the amplitude of the vibration of the stator has a peak shape. This leads to the distribution of the normal compressive stress with a very larger amplitude, which based on (15) when P holds a constant. Due to the large amplitude of the normal compressive force between the contact surface, it only needs a short contact length to balance the compressive force. So the contact length sharply reduces when the frequency is near to the resonant frequency of the motor system, and there is a notch shape of the contact length. Therefore, it is concluded that the contact stiffness only has a small

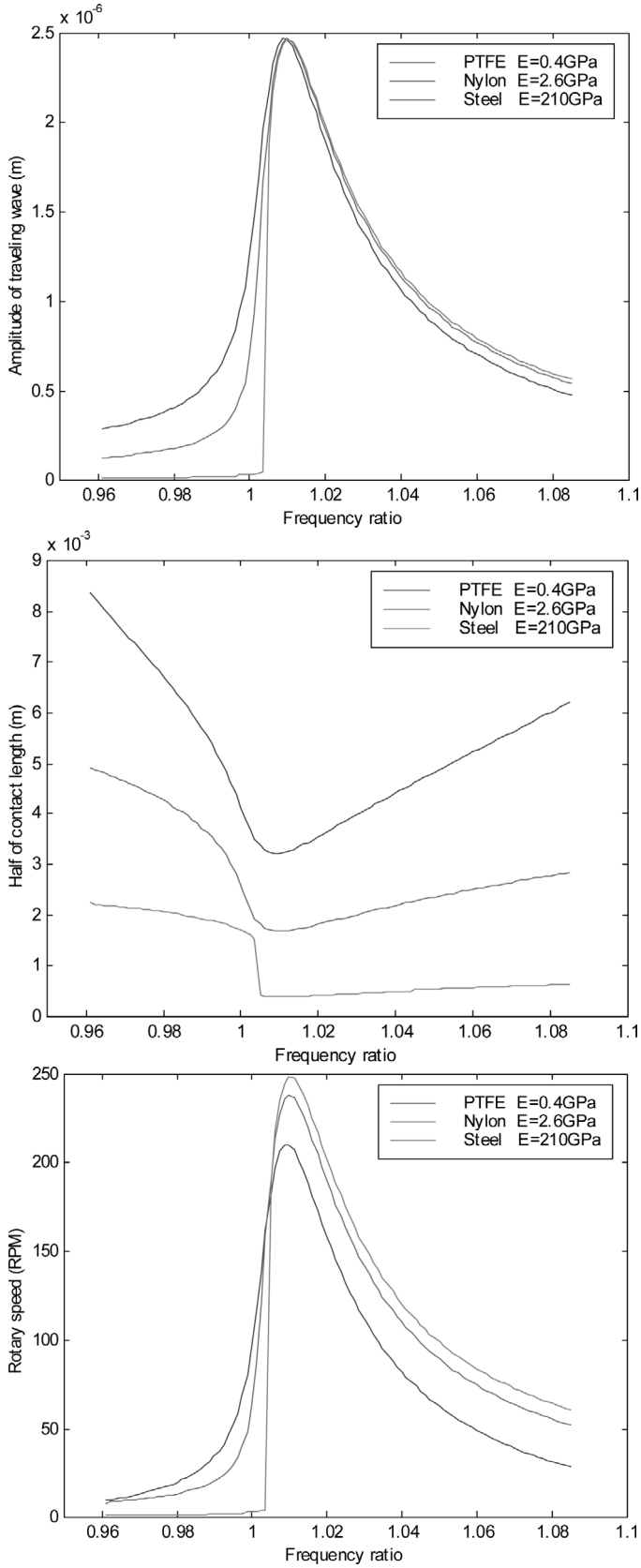

Fig. 4. Top, Amplitude of the traveling wave in the stator. Center, Half of the contact length between the stator and the rotor. Bottom, Frequency response of the motor for different contact layer materials where $P = -80$ N, $M_{\text{applied}} = 0.15$ Nm, $V = 150$ V, $h_c = 0.5$ mm, $\mu = 0.18$, and $\zeta = 1\%$.

effect on the stator vibration system due to a small shift of the peak and the lower the Young's modulus, the longer the contact length and the lower the rotation speed of the motor. The phenomenon can be explained by means of the contact stiffness. It is well-known that the lower the Young's modulus, the lower the contact stiffness. So the contact layer with a lower Young's modulus has a larger contact length under the action of the same compressive force. Therefore, in order to balance the external load, a longer contact length results in a lower speed of the rotor. This can be interpreted by the distribution of the tangential velocities of the stator and rotor, shown in Fig. 2. At points A and B, the speed of rotor is equal to the speed of stator. Due to the different relative speed between the stator and rotor, zones I, II, and III have different directions of frictional forces. In the zones I and III, the speed of the rotor is larger than the speed of the stator. The frictional forces F_I and F_{III} are opposite to the direction of the rotor speed. In zone II, the speed of the rotor is less than the speed of the stator. The frictional force F_{II} has the same direction as the rotor speed. Under the action of external load F_e, the balance equation of the forces is that $\mathrm{F}_e = \mathrm{F}_{II} - \mathrm{F}_I - \mathrm{F}_{III}$ for the contact surface. Under the action of the same external force and even $\mathrm{F}_e = 0$, in order to remain the balance equation, a longer contact length causes points A and B to move toward points C and D, respectively. So a longer contact length results in a lower speed of the rotor. It should be mentioned that the friction coefficient is strongly related to different contact layer material. But here, in order to discuss the influence of the contact layer stiffness on motor performance, the friction coefficient is taken to be a constants.

The load response of the motor for different contact layer material has been simulated. The motor speed versus external applied loads is shown in Fig. 5, where P, V, h_c, μ, and ς are taken as -80 N, 150 V, 0.5 mm, 0.18, and 1%, respectively. Again, it is observed that the contact-layer material has a great effect on the speed-load characteristic of the motor. When using material with a low Young modulus, the motor has a soft, speed-load characteristic. For a high value of Young modulus, the motor has a hard, speed-load characteristic. Therefore, taking all these considerations into account, the choice of the contact-layer material should be based not only on the maximum permissible compressive force of the motor, but also on the frequency response and the load characteristics of the motor.

C. Influence of the Thickness of the Contact Layer on Motor Performance

In order to understand the influence of the thickness of the contact layer on motor performance, the load response of the motor at different contact-layer thickness has been simulated. The motor speed verse external load applied is shown in Fig. 6, in which the contact-layer material is nylon and the parameters of P, V, ω, μ, and ς are taken to be the same as in Fig. 5. From Fig. 6, it is observed that the

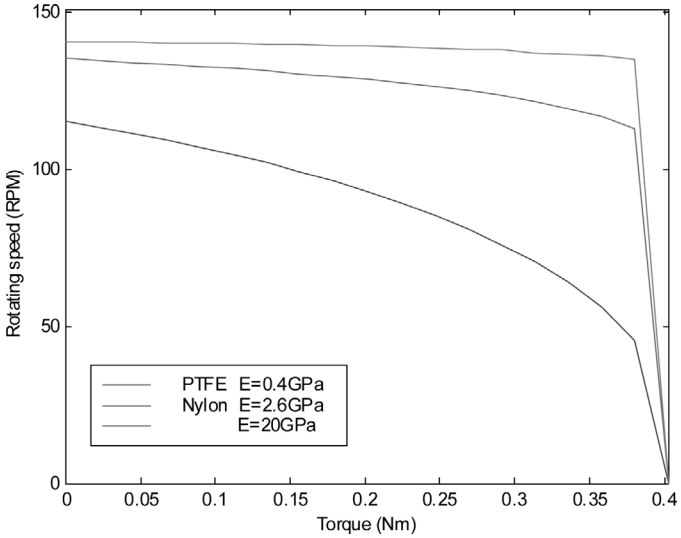

Fig. 5. Motor speed against external loads applied for different contact layer material where $P = -80$ N, $V = 150$ V, $\omega = 1.0355\omega_n$, $h_c = 0.5$ mm, $\mu = 0.18$, and $\zeta = 1\%$.

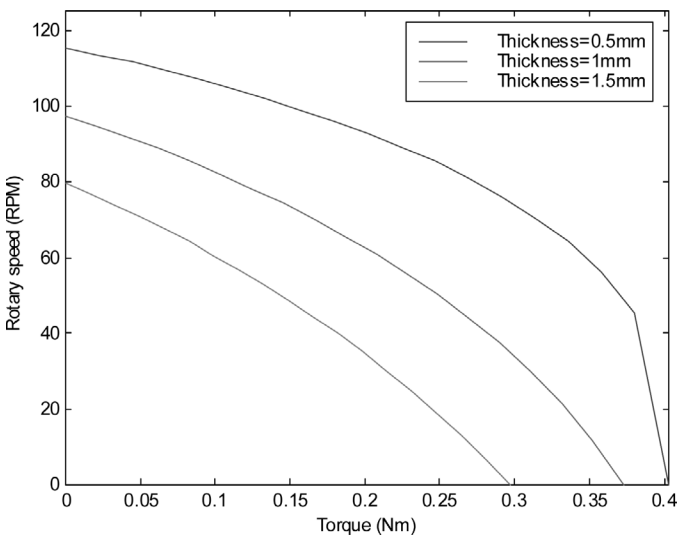

Fig. 6. Load response of rotation speed of the rotor for different thickness of the contact layer where the contact-layer material is PTFE, $P = 80$ N, $V = 150$ V, $\omega = 1.0355\omega_n$, $h_c = 0.5$ mm, $\mu = 0.18$, and $\zeta = 1\%$.

contact-layer thickness not only has a great effect on the rotation speed of the rotor, but also on the stall torque of the motor. The thinner the contact layer, the higher the no-load speed of the rotor and the stall torque. Therefore, within the imposed limit by machining, the contact layer should be designed to be as thin as possible to maximize the motor performance. The reason for this is that a thinner contact layer has a higher contact stiffness and a shorter contact length. This results in a higher speed of the rotor.

D. Influence of the Compressive Force on Motor Performance

The TWUM usually work at or near the resonant frequency of the motor and can have better performance.

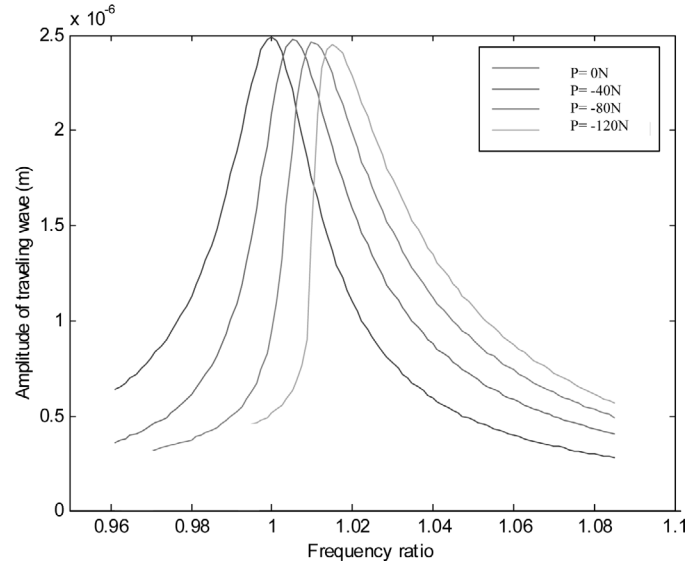

Fig. 7. Frequency response of the amplitude of the traveling wave of the stator for different compressive forces in which the material contact layer is PTFE, $E = 0.4$ GPa, $M_{\text{applied}} = 0.15$ Nm, $V = 150$ V, $h_c = 0.5$ mm, $\mu = 0.18$, and $\zeta = 1\%$.

For example, the motor is able to receive a larger input power and output high speed and high torque for a given input voltage. But the compressive force causes the resonant frequency of the motor change. For this reason, it is very valuable to find the resonant frequency of the motor under a compressive force.

The frequency responses of the motor for different compressive force have been simulated, and the amplitude of the traveling wave of the stator is shown in Fig. 7, in which the contact-layer material is PTFE and the parameters of $\mathrm{M}_{\text{applied}}$, V, h_c, μ, and ς are taken to be the same as in Fig. 4. In Fig. 7, the peak position of P being equal to zero corresponds to the resonant frequency of the stator with piezoceramics, and the peak positions of P not being equal to zero correspond to the resonant frequencies of the motor under different compressive force. Especially emphasizing here, the resonant frequency of the motor under the compressive force is not the resonant frequencies of the stator because the compressive force changes the resonant frequency of the motor. However, the resonant frequency of the stator usually is tested and used for the driving frequency, although it is not the resonant frequency of the motor. The main reason is that most measurement instruments of vibration only allow input a small signal to excite measured systems. If using the instruments to measure the resonant frequency of the motor under action of a practical compressive force of the motor, the compressive force would completely suppress the small vibration excited by the small signal. So, using the resonant frequency of the stator instead of the resonant frequency of the motor for the time being. How to measure the resonant frequency of the motor under a larger compressive force is an open question and needs to be solved in the future. From this point, it seems more valuable for using the present model to predict the resonant frequency. Further-

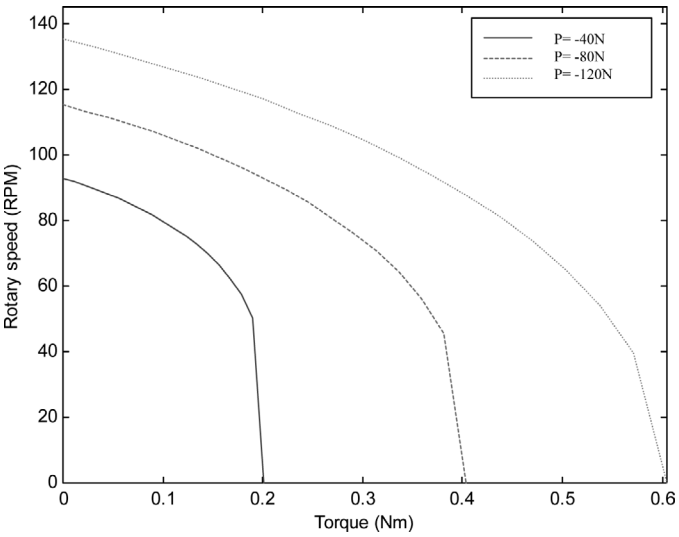

Fig. 8. Load response of the motor for different compressive forces in which the contact-layer materials is PTFE, $E = 0.4$ GPa, $V = 150$ V, $\omega = 1.0355\omega_n$, $h_c = 0.5$ mm, $\mu = 0.18$, and $\zeta = 1\%$.

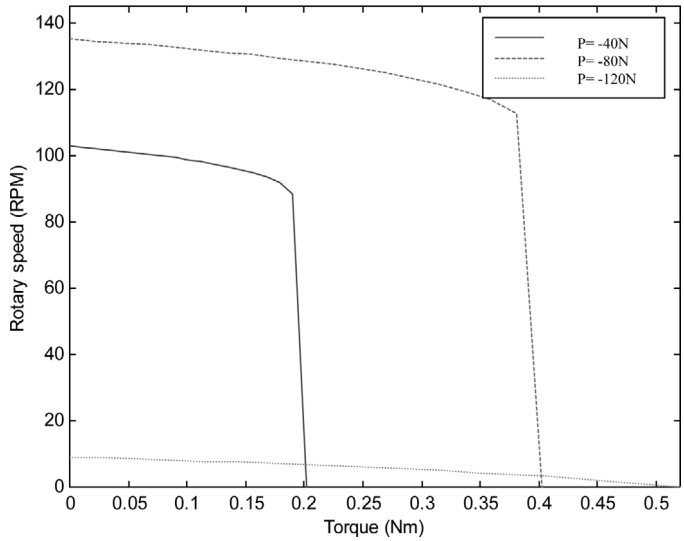

Fig. 9. Load response of the motor for different compressive forces in which the contact-layer material is nylon, $E = 2.6$ GPa, $V = 150$ V, $\omega = 1.0355\omega_n$, $h_c = 0.5$ mm, $\mu = 0.18$, and $\zeta = 1\%$.

more, from Fig. 7, another two features can be observed. With the increase of the compressive force, the curve on the left-hand side of the peak frequency more dramatically steepens and the pull-out phenomenon is exhibited. The pull-out phenomenon is referred to the curve of the left-hand side is steeped and the curve of the right-hand side becomes more gradual with the increase of the frequency. It is not clear what causes the pull-out phenomenon. But the author thinks that the nonlinear characteristic of the motor system causes this. It is well-known that there is a jump phenomenon in strong nonlinear systems. Due to the appearance of the contact force in the governing equation in (15), the motor system is a nonlinear system. The larger the contact force, the stronger the pull-out phenomenon. The larger the compressive forces, the larger the amplitude of traveling waves of the stator at the same excitation frequency on the right-hand side of the peak frequency. Therefore, in an allowable range, the compressive force should be applied to be as large as possible, and the excitation frequency chosen to be on the right-hand side of the peak frequency.

The load responses of the motor for different compressive forces have been simulated and shown in Fig. 8, in which the contact-layer material is PTFE, the contact lengths are all less than half the wavelength, and the parameters V, ω, h_c, μ, and ς are taken to be the same as in Fig. 5. From Fig. 8, two features can be observed. No-load speed of the motor increases with an increase of the compressive force. This can be understood and explained by means of the amplitude of the traveling wave of the stator. The reason is that the amplitude of the traveling wave in the steady state becomes larger with an increase of the compressive force. The stall torque increases proportionally with the compressive force. It is noted that the conclusion is true only if the contact length is less than half wavelength. Otherwise, it is false. Furthermore, in order to show the false, the case is simulated that the contact length is larger than half wavelength when P = 120 N. The load response of the motor for different compressive forces is shown in Fig. 9, in which the parameters of V, ω, h_c, μ, and ς are taken to be the same as in Fig. 5 and the contact-layer material is nylon. From Fig. 9, it is observed that the no-load speed of the motor first increases with the compressive force, then dramatically decreases with the increase of the compressive force, and the stall torque is not proportional to the compressive force in the case of P = 120 N because the contact length is over half wavelength.

VII. Conclusions

This paper focuses on a contact analysis of TWUM and incorporates the analysis into the model previously studied by Hagood for a proper choice and design of contact-layer material and parameters and for understanding how the compressive force governs motor performance. The model here differs from the Hagood's model. A new contact analysis model is proposed. The steady-state solution to the nonlinear governing equations of motion of the stator is derived in the frequency domain, rather than in the time domain. The present model can predict some special characteristics and behavior of the motors, including the maximum compressive force of the motor, the starting-up voltage, the stall torque, the pull-out phenomenon, the resonant frequency of the motor under the action of the compressive force, and the effect of the contact-layer material and the thickness of the contact layer on the motor characteristics.

By use of the proposed model, a series of frequency response and operational characteristics of the motor performance have been simulated. The influences of the contact-layer material, the thickness, and the compressive force

on the motor performance are discussed and physically interpreted. They are useful to understand the influence of the compressive force and contact-layer material on motor performance. They also are used for a prior calculation of motor characteristics, such as no-load speed, stall torque, maximum permissible compressive force, starting-up voltage, natural frequency, input power, output power, and efficiency. However, the present model does not take into account the effect of the tangential forces on the stator vibration and does not consider the viscoelastic behavior of the contact layer and the variation of the dynamic friction versus the axial preload and sliding speed. In spite of these deficiencies, the present model is a step forward, a further development in analyzing the contact layer and so will be of assistance in the design of the TWUM with high performance.

Acknowledgments

This work was performed with the support of the Alexander von Humboldt Foundation of Germany. The author would like to thank the support. The author also would like to thank Paul Kirby and Robert Wright's useful suggestion.

References

[1] K. Uchino, "Piezoelectric ultrasonic motor: Overview," *Smart Mater. Struct.*, vol. 7, no. 1, pp. 273–285, 1998.
[2] K. Uchino, *Piezoelectric Actuator and Piezoelectric Motors.* Boston: Kluwer, 1997.
[3] S. Ueha and T. Tomikawa, *Piezoelectric Motor: Theory and Application.* Oxford: Clarendon, 1993.
[4] T. Shashida and T. Kenjio, *Introduction to Piezoelectric Motor.* Oxford: Clarendon, 1993.
[5] H. Hirata and S. Ueha, "Design of a traveling wave type ultrasonic motor," *IEEE Trans. Ultrason., Ferroelect., Freq. Contr.*, vol. 42, no. 2, pp. 225–231, 1995.
[6] Y. Kagawa and G. M. L. Gladwell, "Finite element analysis of flexure-type vibration with electrostrictive transducers," *IEEE Trans. Sonics Ultrason.*, vol. 17, no. 1, pp. 41–49, 1970.
[7] T. Yamabushi and Y. Kagawa, "Numerical simulation of a piezoelectric ultrasonic motor and its characteristics," *J. Jpn. Soc. Simul. Technol.*, vol. 8, pp. 69–76, 1989.
[8] Y. Kagawa, T. Tsuchiya, T. Yamabushi, and T. Furukawa, "Finite element simulation of dynamic responses of piezoelectric actuators," *J. Sound Vib.*, vol. 191, no. 4, pp. 519–538, 1996.
[9] T. Maeno and A. Miyaka, "Finite element analysis of the rotor/stator contact in a ring type ultrasonic motor," *IEEE Trans. Ultrason., Ferroelect., Freq. Contr.*, vol. 39, no. 4, pp. 668–674, 1992.
[10] M. Nakamura, H. Kurebayashi, and S. Ueha, "An estimation of load characteristics of an ultrasonic motor by measuring transient response," *IEEE Trans. Ultrason., Ferroelect., Freq. Contr.*, vol. 38, no. 5, pp. 481–485, 1991.
[11] P. Hagedorn and J. Wallaschek, "Traveling wave ultrasonic motors. Part I: Working principle and mathematical modeling of the stator," *J. Sound Vib.*, vol. 155, no. 1, pp. 31–46, 1992.
[12] A. M. Flynn, "Piezoelectric ultrasonic micromotors," Ph.D. dissertation, Department of Electrical Engineering and Computer Science, Massachusetts Institute of Technology, Cambridge, MA 1995.
[13] O. Y. Zharii, "An exact mathematical model of a traveling wave piezoelectric motor," in *Ultrason. Symp.*, 1994, pp. 545–548.
[14] O. Y. Zharii, "Adhesive contact between the surface wave and a rigid strip," *Trans. ASME J. Appl. Mech.*, vol. 62, no. 2, pp. 368–372, 1995.
[15] O. Y. Zharii and A. F. Ulitko, "Smooth contact between the running Rayleigh wave and a rigid strip," *Trans. ASME J. Appl. Mech.*, vol. 62, no. 2, pp. 362–367, 1995.
[16] N. W. Hagood, IV and J. M. Andrew, "Modeling of a piezoelectric rotary ultrasonic motor," *IEEE Trans. Ultrason., Ferroelect., Freq. Contr.*, vol. 42, no. 2, pp. 210–224, 1995.
[17] P. Hagedorn, T. Sattel, D. Speziari, and G. Diana, "The importance of rotor flexibility in ultrasonic traveling wave motors," *Smart Mater. Struct.*, vol. 7, no. 3, pp. 352–368, 1998.
[18] M.-L. Zhu, "The research on piezoelectric traveling wave piezoelectric motor," *Postdoctoral Investigated Report of Nanjing University of Aeronautics and Astronautics*, Nanjing, China, 1996.
[19] Y. Kagawa and T. Yamabushi, "Finite approach for a piezoelectric circular rod," *IEEE Trans. Sonics Ultrason.*, vol. 23, Suppl. 6, pp. 379–385, 1976.
[20] Y. Kagawa and Y. Yamabushi, "Finite element simulation of a composite piezoelectric ultrasonic transducer," *IEEE Trans. Sonics Ultrason.*, vol. 23, Suppl. 2, pp. 81–88, 1979.
[21] D. Boucher, M. Lagier, and C. Maerfeid, "Computation of the vibrational modes for piezoelectric array transducers using a mixed finite element-perturbation method," *IEEE Trans. Sonics Ultrason.*, vol. 28, Suppl. 5, pp. 144–153, 1981.
[22] K. Yong and Y. Cho, "Algorithms for eigenvalue problems in piezoelectric finite element analyses," in *Ultrason, Symp.*, 1994, pp. 1057–1062.
[23] H. Hirata and S. Ueha, "Force factor design of disk vibrators used for piezoelectric motors," *J. Acoust. Soc. Jpn. (E)*, vol. 13, no. 2, pp. 77–84, 1992.
[24] J. Maas, P. Ide, N. Frohleke, and H. Grotstollen, "Simulation model for ultrasonic motors powered by resonant converters," in *IEEE Industry Appl. Conf.*, 1995, pp. 111–120.
[25] J. Maas, T. Schulte, and H. Grotstollen, "Optimized drive control for inverter-fed ultrasonic motors," in *IEEE Industry Appl. Conf.*, 1997, pp. 690–698.
[26] K. L. Johnson, *Contact Mechanics.* New York: Cambridge Univ. Press, 1999, pp. 368–372.
[27] V. Z. Parton and B. A. Kudryavtsev, *Electromagnetoelasticity.* New York: Gordon and Breach Sci. Publ., 1988.

Meiling Zhu received her B.S., M.S., and Ph.D. of Eng. degrees from Southeast University, Nanjing, China, in 1989, 1992, and 1994, respectively. From 1995 to 1996, she was a postdoctor at the Institute of Vibration Engineering Research (IVER), the Nanjing University of Aeronautics and Astronautics (NUAA). Beginning in 1997, she was an associate professor in the IVER, NUAA. She was with the Department of Mechanical Engineering, the Hong Kong University of Science and Technology from 1998 to 1999. From 1999 to 2001, she was a research fellow of the Alexander von Humboldt Foundation at the Institute B für Mechanik, Stuttgart Universität, Stuttgart, Germany. She then was a research fellow in the School of Mechanical Engineering, the University of Leeds, Leeds, England, UK.

Currently, Dr. Zhu is a research officer of the School of Industrial and Manufacturing Science at Cranfield University, Bedfordshire, England, UK.

She has contributed to numerous technical publications in various research areas. Her research activities include smart material and structures, piezoelectric ultrasonic motors, microelectromechanical systems (MEMS), and MEMS sensors and actuators, thin-film bulk acoustic wave resonators and filters, and microwave devices.

Cranfield University

CERES Research Repository **https://dspace.lib.cranfield.ac.uk/**

School of Applied Sciences (SAS) (2006-July 2014) Staff publications (SAS)

Contact Analysis and Mathematical Modeling of Traveling Wave Ultrasonic Motors

Zhu, Meiling

2004-11-01T00:00:00Z

IEEE Transaction on Ultrasonics, Ferroelectrics and Frequency Control, 51(6), June 2004, p.668-679
http://dx.doi.org/http://dx.doi.org10.1109/TUFFC.2004.1304265

Downloaded from CERES Research Repository, Cranfield University